This is a repository copy of *Coupled element and structural level optimisation framework for cold-formed steel frames*.

Article:

Phan, D.T., Mojtabaei, S.M. orcid.org/0000-0002-4876-4857, Hajirasouliha, I. orcid.org/0000-0003-2597-8200 et al. (2 more authors) (2020) Coupled element and structural level optimisation framework for cold-formed steel frames. Journal of Constructional Steel Research, 168. 105867. ISSN 0143-974X

Coupled Element and Structural Level Optimisation Framework for Cold-Formed Steel Frames

Duoc T. Phan [1], Seyed Mohammad Mojtabaei [2*], Iman Hajirasouliha [2], Jun Ye [3], James B.P. Lim [4]

[1]Department of Civil Engineering, Faculty of Engineering and Science, University of Nottingham Malaysia

[2]Department of Civil and Structural Engineering, The University of Sheffield, Sheffield, UK

[3]Department of Civil and Environmental Engineering, Imperial College London, London, UK

[4]Department of Civil and Environmental Engineering, The University of Auckland, Auckland, New Zealand

* Corresponding author: smmojtabaei1@sheffield.ac.uk

Abstract

Optimisation of cold-formed steel (CFS) structures can be challenging due to the complex behaviour of thin-walled CFS sections affected by different buckling modes. In this paper, a coupled framework is presented for element and structural level optimisation of CFS portal frames, under serviceability limit state (SLS) and ultimate limit state (ULS) conditions, using Genetic Algorithm. First, CFS lipped-channel beam sections are optimised with respect to their flexural capacity determined in accordance with the effective width method specified in Eurocode 3 (EC3). The relative dimensions of the cross-section are considered as the main design variables, while the EC3 plate dimensions and slenderness limits and a number of manufacturing and end-use constraints are taken into account in the optimisation process. The results show that the optimum CFS sections exhibit significantly higher (up to 84%) ultimate capacity compared to the standard lipped channel sections with the same plate width and thickness. The structural level optimisation is then carried out to obtain the optimal design solution for a long-span CFS portal frame with knee braces under SLS and ULS conditions. Compared to conventional optimisation using standard cross-sections, it is shown that the proposed coupled framework leads to more cost-effective solutions (up to 20% less structural material) by using the more efficient CFS cross-sectional shapes optimised for generic applications. The results also indicate that optimising the frame geometry and knee brace configuration can noticeably improve the structural performance and reduce the required structural weight, especially when both ULS and SLS conditions are considered.

Keywords

Cold-Formed Steel (CFS); Portal frame; Optimisation; Effective width; Serviceability Limit State (SLS); Ultimate Limit State (ULS)

1 Introduction

Cold-formed steel (CFS) sections are increasingly used in construction practice due to their advantages such as a relatively high strength-to-weight ratio, greater flexibility in manufacturing, and ease of handling, transportation and installation. The flexibility of CFS cross-sectional shapes, through determining optimum

relative dimensions of channel sections (i.e. size optimisation), provides an excellent opportunity to enhance the load-carrying capacity of available standard sections. This enhancement of capacity at the element level may subsequently improve the capacity of the CFS frame system, especially for medium to long-span CFS portal frame buildings.

Optimisation of CFS sections can be a challenging task due to typical manufacturing and end-use design constraints and complex behaviour of CFS elements controlled by combinations of local, global and distortional buckling modes. Several investigations have previously been conducted to optimise predefined standard CFS profiles such as C channels, and I and Z shape beams [1, 2]. The results demonstrated that optimising the cross-sectional geometry of simply-supported CFS beams subjected to uniformly distributed vertical or transverse load can substantially improve their flexural capacity, as compared with standard sections. Ye et al. [3] showed that by simply changing the relative dimensions of standard commercial channels, optimised sections could be obtained with considerably (up to 30%) higher flexural capacities. Based on their study, Fig.1 compares the dimensions of a standard CFS lipped-channel beam section and the section with the same coil width and plate thickness optimised for maximum flexural capacity. In a follow-up study, Ye et al. [4] concluded that the optimisation on unbraced CFS beams with different lengths could offer up to 75% higher flexural strength compared to using standard sections. Gilbert et al. [5] and Wang et al. [6] adopted Genetic Algorithm (GA) and Augmented Lagrangian methods to minimise the required material to achieve the same level of strength in CFS column and beam-column members, respectively. Leng et al. [7, 8] optimised the shape of CFS columns for maximum compressive capacity using and unconstraint optimisation methods. It was demonstrated that by restricting the cross-sectional shape to pre-determined elements, the capacity of the optimised designs may drop significantly compared to unconstrained optimum solutions. In another relevant study, Tran et al. [9] presented a global optimisation technique using the trust-region method (TRM) for designing the cross-section of channel beams subjected to uniformly distributed transverse loading based on the yielding strength, deflection limitation, and different instability modes.

(a) Standard section   (b) Optimised section
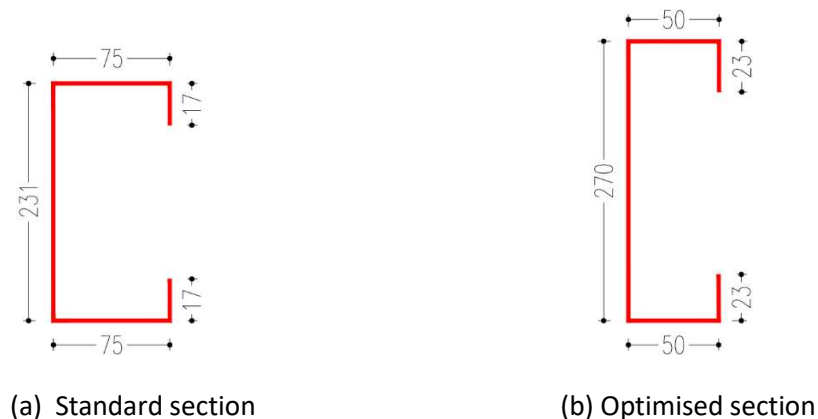
Fig. 1. An example of optimised vs standard CFS lipped-channel beam sections with 1.5 mm plate thickness proposed by Ye et al. [3]

More recently, Mojtabaei et al. [10] adopted Big Bang-Big Crunch (BB-BC) algorithm to obtain optimum CFS beam sections at serviceability limit state (SLS) and ultimate limit state (ULS) conditions. They showed that, for the same amount of material, the flexural capacity and stiffness of optimum CFS beams could be increased by up to 58% and 44%, respectively, compared to their standard counterparts. Using GA optimisation method, Parastesh et al. [11] optimised symmetrical CFS beam-column members by considering practical and manufacturing constraints. It was observed that increasing the eccentricity of the axial load generally leads to more spread sections especially in shorter members. Ye et al. [12] also proposed an advanced shape optimisation framework to achieve maximum energy dissipation of CFS sections in uniaxial bending by providing a link between detailed nonlinear Finite Element (FE) analyses and Particle Swarm Optimisation (PSO) algorithm.

It should be noted that all of the above-mentioned studies were limited to the element level optimisation, and therefore, the effect of using optimised sections on the overall structural behaviour of a building has not been investigated in CFS. While optimum design of CFS elements has been extensively investigated in the past, considerably less research has been conducted on optimisation of CFS structural systems. In one of the few studies available in this area, Phan et al. [13, 14] used Genetic Algorithm (GA) to optimise CFS portal frames with small to medium spans and reported a variation of optimal geometry in terms of pitch and frame spacing for a range of typical column heights. In a follow-up study, it was shown that by taking into account the effects of stressed-skin action (owing to the stiffening effect of roof diaphragm) in the optimisation process, the material cost of the CFS portal frame structural system can be noticeably (up to 53%) reduced [15]. Similar studies on hot-rolled steel portal frames reached a similar conclusion and demonstrated that such frame systems were controlled by serviceability limits [16, 17].

As mentioned above, several studies have been conducted either on the optimisation of cross-sectional dimensions of CFS sections or on the geometry of the CFS frames. However, currently there is no study available to couple these two optimisation levels. It should be noted that for practical applications the simultaneous optimisation of cross-sectional dimensions and the geometry of the structural system is too computationally expensive. To address this issue, a novel methodology is proposed to simplify this complex optimisation process by coupling the element and structural level optimisations. The CFS elements are first optimised for a range of element length, plate thickness and coil width under different uniform distributed load (UDL) levels (continues optimisation). The optimised elements are then used as structural components of the frame to obtain the best design solution under different serviceability limit state (SLS) and ultimate limit state (ULS) conditions (discrete optimisation), while the optimisation solver simultaneously searches through a practical range of values for the roof pitch, frame spacing, and knee brace configuration (i.e. knee depth and knee angle). It is shown that using this innovative approach can significantly reduce the computational cost required for simultaneous optimisation of CFS elements and geometry of the structural systems.

At element level, a practical procedure is presented for the development of conventional CFS back-to-back lipped-channel beam sections with maximum flexural strength by taking into account local, distortional and global buckling modes. To provide a comprehensive range of optimum sections suitable for CFS portal frames, CFS beam members with different span lengths subjected to various levels of uniformly distributed loads (UDLs) are considered in this study. A Genetic Algorithm (GA) program is developed in MATLAB [18] to find the optimum shape of CFS beam members designed according to European design guidelines [19-21] by considering the relative cross-sectional dimensions as main design variables. The EC3 geometrical requirements, as well as a number of practical and manufacturing constraints, are also included in the optimisation process. The efficiency of the proposed optimum CFS cross-sections is then investigated compared to standard commercially available back-to-back sections. At structural level, a long span CFS portal frame with knee braces subjected to different serviceability limit state (SLS) and ultimate limit state (ULS) design load combinations is first analysed using Finite Element (FE) ANSYS software [22] to determine elements' internal forces and lateral displacement of the joints. Subsequently, the GA program is adopted to find the best design solution (i.e. with minimum structural weight) by using standard and optimum CFS sections and considering a set of predefined structural design constraints. The results are then used to assess the efficiency of the proposed coupled framework and to investigate the influence of knee brace configuration on the structure performance of the optimised frame.

2 Design of CFS elements

The structural elements of CFS portal frames are designed in accordance with EC3, taking into account ultimate limit state (ULS) and serviceability limit state (SLS) conditions. This section first presents a brief description of effective width method, used to calculate the buckling resistance of the CFS sections at ULS, following the provisions of EC3 Part 1-3 [20] and EC3 Part 1-5 [21]. The design procedure of CFS members at ULS is then provided to take into account the effect of length based on the provisions of EC3 Part 1-1 [19]. Finally, SLS checks, which are used to control the deflection of the designed CFS members, are briefly described. While it is more accurate to consider the column and beam elements as built-up members [23], the interactions between the back-to-back channels were neglected in this study for the sake of simplicity and providing more conservative design solutions.

2.1   Ultimate Limit State (ULS) design

2.1.1   *Buckling resistance of the cross-section*

2.1.1.1   *Local buckling*

In Eurocode 3 (EC3), the effect of local buckling is considered through the effective width concept. It is based on the observation that local buckling causes a loss of compressive stiffness in the centre of a plate supported along both longitudinal edges (labeled an 'internal' plate element), or along the free edge of a plate supported along one longitudinal edge (an 'outstand' element) as a result of non-linear effects. The

corner zones of the cross-section consequently become the main load-bearing areas. This implied that the local buckling causes the centroid of the effective cross-section to shift over a distance e_N relative to the original centroid of the gross cross-section. As an instance, the effective area of a sample cross-section under major axis pure bending moment is shown in Fig. 2, which is highlighted in solid black lines. According to EC3 Part 1-5 [21], the effective widths of internal and outstand compression elements are given by:

$$\rho = \frac{b_e}{b} = \begin{cases} \dfrac{1}{\lambda_l}\left(1 - \dfrac{0.055(3+\psi)}{\lambda_l}\right) & \text{for interal compression element} \\[3mm] \dfrac{1}{\lambda_l}\left(1 - \dfrac{0.188}{\lambda_l}\right) & \text{for outstand compression element} \end{cases} \tag{1}$$

where:

$$\lambda_l = \sqrt{\frac{f_y}{\sigma_{cr}}} \tag{2}$$

In Eq. 1, ρ is the reduction factor on the plate width, while b and b_e are the total and the effective width of the plate, respectively. The slenderness ratio λ_l relates the material yield stress f_y to the elastic local buckling stress of the plate σ_{cr} and ψ is the ratio of the end stresses in the plate. It should be noted that EC3 Part 1-3 [20] stipulates an iterative process to calculate the effective width of the cross-section since the neutral axis of the effective cross-section shifts over a distance. This affects the stress distribution due to loss of effective section in the flanges and the web. Although not required by EC3 Part 1-3 [20] guidelines, full iterations to convergence are carried out in this study.
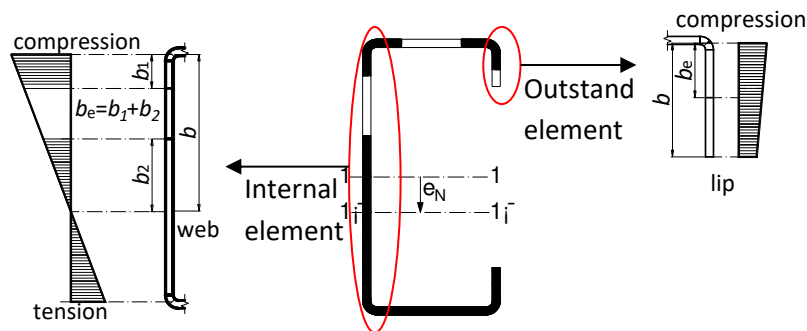
Fig. 2. Effective width of the lipped-channel section based on EC3 [20]

2.1.1.2   Distortional buckling

Distortional buckling describes the distortion of the cross-section with rotation and translation at interior elements, leading to both in-plane and out-of-plane displacements of constituent plates. EC3 takes into account the local buckling and distortional buckling of CFS sections by reducing the effective width and the effective thickness of the constituent plates, respectively. The distortional slenderness, λ_d, can be

calculated based on a simplified model, in which the restraining effects of the adjacent plates in the cross-section are taken into account by using equivalent elastic springs as shown in Fig. 3:

$$\lambda_d = \sqrt{f_y / \sigma_{cr,s}} \qquad (3)$$

where $\sigma_{cr,s}$ is the elastic buckling stress of the plate-stiffener assembly given by:

$$\sigma_{cr,s} = \frac{2\sqrt{KEI_s}}{A_s} \qquad (4)$$

In the above equation, K and A_s are the stiffness of the spring (per unit length) and the effective cross-sectional area of the stiffener, respectively. E is the Young's modulus and I_s is the moment of inertia of the stiffener about the centroid parallel to the plate element. K is a function of the flexural stiffness of the adjacent plates and can be calculated based on the deflection of the stiffener assembly under a unit load $u = 1$ (per unit length).
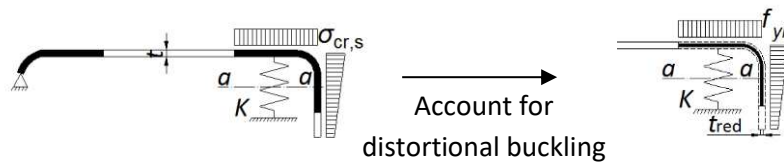
Fig. 3. Simplified models for distortional buckling of flange for CFS lipped-channel section [21]

EC3 also recommends to use an iterative process to update the local slenderness ratio of the plates, λ_l, by replacing $\lambda_{l,red} = \lambda_l \sqrt{\chi_d}$. χ_d is the reduction factor corresponding to the distortional buckling resistance and can be calculated by using the relative slenderness λ_d. For the calculation of λ_d, f_y should be substituted by $\sigma_{com} = \chi_d \cdot f_y$ in each iteration. This optional iteration loop was considered in this study until $\chi_{d,n} \approx \chi_{d,(n-1)}$.

2.1.1.3   Cross-section check

Based on EC3 part 1-3 [20], CFS cross-sections subjected to combined axial compression N_{Ed} and bending moments $M_{y,Ed}$ should satisfy the following criterion:

$$\frac{N_{Ed}}{N_{c,Rd}} + \frac{M_{y,Ed} + \Delta M_{y,Ed}}{M_{cy,Rd,com}} \leq 1 \qquad (5)$$

In the above equation, $N_{c,Rd} = \dfrac{A_{eff} f_{yb}}{\gamma_{M_0}}$ is the design capacity resistance of the cross-section. A_{eff} is the

effective area of the cross-section obtained by assuming a uniform compressive stress $\sigma_{com,Ed} = \dfrac{f_{yb}}{\gamma_{M_0}}$, and

f_{yb} is the basic yield strength. Additional moment $\Delta M_{y,Ed}$ due to the shift of the effective centroidal axes

can be calculated as:

$$\Delta M_{y,Ed} = N_{Ed}.e_N \tag{6}$$

2.1.2   Buckling resistance of the member

2.1.2.1   Knee brace member

The design buckling resistance of a compression member with Class 4 cross-section is given by EC3:

$$N_{b,Rd} = \dfrac{\chi A_{eff} f_y}{\gamma_{M_1}} \tag{7}$$

where A_{eff} is the effective area of the cross-section and χ is the reduction factor for the relevant

buckling mode [19]. Reduction factor (χ) is determined using a minimum of reduction factors for flexural

buckling, torsion buckling, and flexural-torsional buckling modes.

2.1.2.2   Beam-column member

According to EC3, the design of CFS beam-column members requires the calculation of slenderness for

various global buckling modes, defined as:

$$
\begin{cases}
\lambda = \sqrt{\dfrac{A_{eff} f_y}{N_{cr}}} & \text{slenderness for flexural, torsional, and flexural torsional} \\[4mm]
\lambda_{LT} = \sqrt{\dfrac{W_{eff} f_y}{M_{cr}}} & \text{slenderness for lateral-torsional}
\end{cases}
\tag{8}
$$

where N_{cr} is the elastic axial critical compressive load, W_{eff} is the effective section modulus, and M_{cr}

is the elastic lateral-torsional buckling moment based on the gross cross-section. It is worth noting that EC3

Part 1.1 [19] implicitly considers the effects of element length and uniform distributed load on the lateral-

torsional buckling resistance. For slenderness $\lambda_{LT} \leq 0.4$ or for $M_{y,Ed}/M_{cr} \leq 0.16$, lateral-torsional

buckling effects may be ignored and only cross-sectional checks are required.

2.1.2.3   Capacity check

The capacity of the frame members in pure axial compression and pure bending moment should be

verified using the Eqs. (9) and (10), respectively:

$$\frac{N_{Ed}}{N_{b,Rd}} \leq 1 \tag{9}$$

$$\frac{M_{y,Ed}}{M_{b,Rd}} \leq 1 \tag{10}$$

where $M_{b,Rd} = \chi_{LT} W_{eff} f_y / \gamma_{M_1}$ is the design lateral-torsional buckling resistance moment. χ_{LT} is the reduction factor to take into account lateral-torsional buckling effects. The Clause 6.2.5(2) of EN1993-1-3 [20] recommends to use the following interaction formula to consider the interaction between axial force and bending moment in beam-column elements:

$$(\frac{N_{Ed}}{N_{b,Rd}})^{0.8} + (\frac{M_{y,Ed}}{M_{b,Rd}})^{0.8} \leq 1 \tag{11}$$

2.2 Serviceability limit state

EC3 part 1-3 [20] stipulates that the properties of the effective cross-section explained in previous sections must be used in all SLS checks for CFS members. The second moment of area of CFS sections can be also estimated by an interpolation between effective and gross cross-sections for the design load combination using the following expression:

$$I_{fic} = I_{gr} - \frac{\sigma_{gr}}{\sigma}(I_{gr} - I(\sigma)_{eff}) \tag{12}$$

where I_{gr} is the second moment of area of the gross cross-section, σ_{gr} is the maximum compressive bending stress based on the gross cross-section at serviceability limit state (SLS), and $I(\sigma)_{eff}$ is the second moment of area of the effective cross-section by considering local buckling estimated based on maximum stress $\sigma \geq \sigma_{gr}$.

3 Design of CFS portal frames

The characteristic values of the gravity actions applied on the proposed CFS portal frame are determined following the provisions of Eurocode 1 [24, 25] by assuming that the frame is located at Belfast, Northern Ireland. The permanent load (*G*) and variable loads (*Q*), including imposed load and snow load, are considered as below:

- Permanent load: 0.15 kN/m² + self-weight of primary steel members
- Snow load: 0.4 kN/m²
- Imposed load: 0.6 kN/m²

The wind load is laterally applied to the CFS frame at both transverse and longitudinal directions in accordance with Eurocode 1, Part 1-4 [26]. The design wind pressures (w) are calculated using the following expression:

$$w = q_P\left(C_{pe} - C_{pi}\right)$$ (13)

where q_p is the peak velocity pressure taken equal to 1.0 kN/m^2, and C_{pe} and C_{pi} are the external and internal pressure coefficients, respectively. It is assumed that the proposed frame is under normal permeability condition without dominant openings, hence C_{pi} possesses the minimum values of -0.3 and +0.2 for negative and positive pressure, respectively. In total, six wind load cases are taken into account in this study [15].

The load combinations at ultimate limit state (ULS) design is adopted from Eurocode 0, Equation 6.10 [27]:

$$\sum_{j\geq1}\gamma_{G,j}G_{k,j} + \gamma_{Q,1}Q_{k,1} + \sum_{i\geq1}\gamma_{Q,i}\psi_{0,i}Q_{k,i}$$ (14)

For the serviceability limit state (SLS) design, Equation 6.14b extracted from Eurocode 0 [27] is used:

$$\sum_{j\geq1}G_{k,j} + P + Q_{k,1} + \sum_{i\geq1}\psi_{0,i}Q_{k,i}$$ (15)

The design load combinations used in this study, including the partial factors and combination factors, are listed in Table 1. It is worth mentioning that the load combinations including imposed action of roofs and either wind or snow load are not considered since it is expected that the permanent action with imposed load or the permanent action with snow load and wind load provide the critical load combinations for ultimate and serviceability limit state designs [25]. In this study, the serviceability checks of the CFS portal frame such as vertical deflection at apex and horizontal displacement at eaves joints are determined based on SCI recommendations [28], in which the lateral displacement of the eaves joint is limited to 1% of column height and the apex vertical deflection limit is considered to be span/200. The serviceability checks are carried out following the SLS load combinations as listed in Table 1.

Table 1. Frame loadings and typical load combinations

Load combinations (LCs)	Permanent actions	Variable actions				
	Partial factor (γ_G)	Leading action		Accompanying action		
		Action	Partial factor (γ_Q)	Action	Partial factor (γ_Q)	Combination factor (ψ_0)
LC1: Permanent & imposed (ULS)	1.35	Imposed	1.5			
LC2: Permanent, snow & wind (ULS)	1.35	Snow	1.5	Wind	1.5	0.5
LC3: Permanent, wind & snow (ULS)	1.35	Wind	1.5	Snow	1.5	0.5
LC4: SLS 1	1.0	Imposed	1.0			
LC5: SLS 2	1.0	Wind	1.0	Snow	1.0	0.5
LC6: SLS 3	1.0	Snow	1.0	Wind	1.0	0.5

4 Frame modelling and analyses

The CFS long-span portal frame considered in this study is based on the full-scale experimental tests conducted by Blum [29, 30]. The main structural components of the CFS portal frame include CFS columns and rafters consisted of back-to-back lipped-channel sections (BBC). In this study, the geometry of the CFS portal frame is expressed in terms of the following design parameters: span length L_f, column height h_f, pitch of frame θ_f, frame spacing (bay) b_f, knee brace length L_k, knee depth d_k, and knee angle θ_k (see Fig. 4). The design parameters for the CFS frame used in the reference experimental tests [29, 30] are: L_f=13.6 m, h_f=5.4 m, θ_f=10°, b_f=3.6 m, L_k=2.68 m, d_k=1.36 m, and θ_k=50°. It is worth noting that more efficient framing system with a given span and column height could be obtained through varying the pitch of frame, frame spacing, and knee brace configuration.
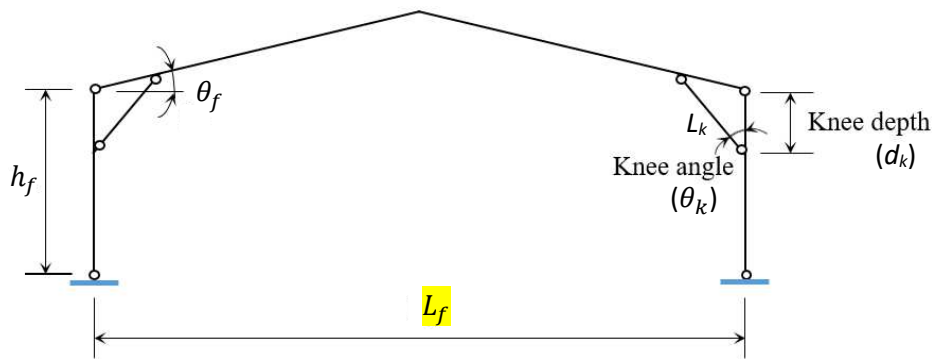
Fig. 4. Geometry of long-span CFS portal frame with knee braces used in this study

In the reference experimental test, all frame members (i.e. columns and rafters) were laterally restrained by using secondary members such as purlins and side rails. Therefore, in this study out-of-plane restraints were applied at 1.3 m intervals along the length of the elements to prevent lateral displacements. The column-to-base connection was assumed to be pinned to the foundation. While the column base connections in the CFS portal frames are generally semi-rigid, the results of the reference experimental frame [29, 30] showed a relatively small bending moment at the column base (around 20% of the moment for fix base columns). This indicates that the responses of the column base connections were closer to the pined connections. It should be also noted that assuming pin column base connections leads to more conservative results especially when serviceability limit state governs the design. Column-to-rafter connections and rafter-to-rafter connections were assembled using eaves and apex joints, respectively, formed through plane brackets bolted between the webs of the channel-sections (Fig. 5). It should be noted that the thickness and depth of the CFS rafter can significantly affect the connection stiffness and strength, leading to a change in the distribution of internal actions and deflections of a portal frame [31].
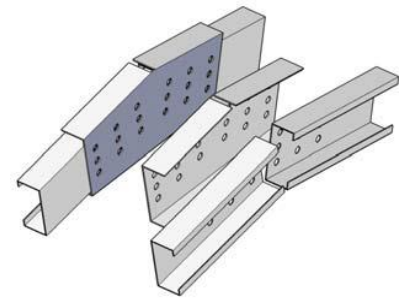
(a) Eaves joint [30]   (b) Apex joint

Fig. 5 Details of frame connections at eaves and apex

Based on the results obtained from the reference experimental tests, column-to-rafter connections, knee-to-column and knee-to-rafter connections can be reasonably considered as pinned joints [29, 30], while moment connections with nine bolts used for apex joints were capable to carry bending moments [32]. It was also reported that rigid apex joints could be efficiently provided in the CFS portal frame by using bolt group length larger than 0.4 m [29, 33]. In this study, it is assumed that the bolt group length is larger than triple of the beam depth, hence the effect of bi-moment caused by the presence of the bolts can be practically neglected [34-36]. Therefore, the buckling resistance of back-to-back channel sections is obtained by assuming that the single channels can buckle individually. It was observed from the experimental test results that a significant bending moment was developed in the columns and rafters at the intersection with the knee braces, while a considerably lower bending moment (up to 50%) was reported in the apex joint [29, 30].

Previous studies have shown that detailed FE models can accurately predict the behaviour of CFS frames under axial and lateral loads (e.g. [37]). In this study, FE model of the reference frame was developed in ANSYS software [22]. To model the CFS columns and rafters, BEAM4 element available in ANSYS library was utilised, while LINK1 element, which can be representative of the axial members, was used for the knee bracing members. Pinned joints were simulated using rotational spring elements with zero length connected to two coincident nodes at the joint positions (COMBIN40). Structural analysis was then conducted to obtain internal forces of the elements and displacements of the joints under the design load combinations explained in the previous section. The effect of geometric nonlinearity (i.e. P-Δ and P-δ) was taken into account using second-order elastic analysis. However, based on the Bernoulli's beam theory, the effect of cross-section warping under shear stress action was neglected. In general, a very good agreement has been achieved between the internal forces of the beams and columns obtained from FE analysis and the experimental test results reported by Blum et al. [29, 30].

5 Optimisation problem

5.1 Cross-section size optimisation

The size optimisation procedure aimed to optimise cross-sectional dimensions of the CFS beam members with regard to their flexural capacity, determined according to the EC3 effective width method (see Section 2). Standard CFS back-to-back lipped-channel sections with steel grade S390 (f_y = 390MPa) were taken as the starting point of the optimisation process. Table 2 lists the utilized standard cross-sections which were selected after consultation with the industrial partner of the project. The elastic modulus and the Poisson's ratio of CFS material were taken as 210 GPa and 0.3, respectively. To provide generic application of optimised CFS sections, simply supported beams subjected to uniformly distributed load (UDL) were considered in this study. The beams were assumed to be laterally braced. The effective length of the lateral restraints, which is identified as the spacing of purlins and side rails, was taken to be 1.3 m. It is worth noting that such spacing of 1.3 m was found to be appropriate for cost-effective design of purlins and side rails [38]. In this case, the optimisation target could be represented as a function of the effective property of the cross-section and the reduction factor for lateral-torsional buckling defined by:

$$\text{Max: } f(x) = \chi_{LT}.W_{eff}.f_y / \gamma_{M_1} \tag{16}$$

$$\text{Subjected to: } \frac{M_{Ed}}{M_{b,Rd}} \leq 1 \tag{17}$$

The reduction factor χ_{LT} was calculated for three typical UDLs of 4.0, 6.0 and 8.0 kN/m, and three different member lengths of 4.0, 6.0, and 8.0 m. It worth mentioning that according to EC3 the reduction factor explicitly considers the effect of imperfections through the cross-sectional buckling curve.

To ensure that the optimum solutions result in practically useful cross-sections, the following EC3 design constraints along with some practical and manufacturing limitations were imposed to the cross-section as listed in Table 3:

a) Similar to standard CFS elements, the overall shape of the cross-section was restricted to a lipped-channel section.

b) The width of the flanges was required to be at least 40mm in order to connect roofing system to the CFS beam elements by screws.

c) The lip had a minimum length of 10 mm to facilitate the CFS forming process. This manufacturing constraint was recommended by the industrial partner of the project.

d) The minimum depth of the channel section was assumed to be 100 mm, which allows a bolted connection or bridging to be constructed. By considering the standard floor depth, the maximum height of the web (beam depth) was also limited to 400 mm.
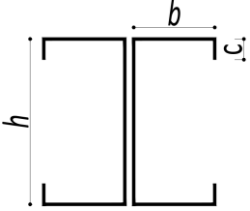
e) The EC3 plate slenderness (width-to-thickness ratio) limits were also considered as design constraints (see Table 3).

It should be noted that the aforementioned constraints, especially in terms of channel dimensions, are typically related to the effect of other elements connected to the CFS beam such as trapezoidal decking, plywood boards and angle cleats. These features are commonly encountered within commercially available sections and do not impose any excessive demands on the fabrication process.

Table 2. Sectional properties of standard CFS back-to-back lipped-channel sections

Section	Depth (mm)	Width (mm)	Lip (mm)	t (mm)	I_y ×10⁶ (mm⁴)	i_{yy} (mm)	I_w ×10⁹ (mm⁶)	I_t (mm⁴)	A_{eff} (mm²)	I_{eff} ×10⁶ (mm⁴)	$W_{y,eff}$ ×10⁴ (mm³)	$M_{b,Rd}$ (kN.m)
C14014	140	62	13	1.4	2.53	56.33	3.34	520.26	382.32	2.05	2.51	9.80
C14015	140	62	13	1.5	2.70	56.28	3.55	639.00	435.37	2.27	2.85	11.10
C14016	140	62	13	1.6	2.87	56.24	3.75	774.42	490.77	2.50	3.20	12.47
C14018	140	62	13	1.8	3.21	56.14	4.13	1099.50	607.83	2.90	3.79	14.78
C14020	140	62	13	2.0	3.54	56.05	4.50	1504.00	726.88	3.29	4.38	17.09
C17014	170	62	13	1.4	3.95	67.00	4.88	575.14	381.96	3.10	3.06	11.92
C17015	170	62	13	1.5	4.22	66.95	5.18	706.50	432.53	3.44	3.46	13.51
C17016	170	62	13	1.6	4.49	66.90	5.48	856.34	486.14	3.78	3.89	15.17
C17018	170	62	13	1.8	5.03	66.80	6.05	1216.20	603.98	4.48	4.79	18.68
C17020	170	62	13	2.0	5.55	66.70	6.59	1664.00	724.54	5.14	5.64	22.01
C17025	170	62	13	2.5	6.85	66.46	7.85	3229.20	1016.00	6.48	7.22	28.18
C20014	200	70	15	1.4	6.30	78.56	9.97	666.61	392.60	4.59	3.71	14.45
C20015	200	70	15	1.5	6.73	78.51	10.59	819.00	445.38	5.10	4.21	16.42
C20016	200	70	15	1.6	7.16	78.46	11.20	992.87	500.74	5.62	4.74	18.47
C20018	200	70	15	1.8	8.02	78.36	12.40	1410.60	620.35	6.70	5.86	22.84
C20020	200	70	15	2.0	8.87	78.26	13.55	1930.70	753.76	7.80	7.06	27.52
C20025	200	70	15	2.5	10.96	78.01	16.24	3750.00	1088.60	10.27	9.71	37.87
C24015	240	74	17	1.5	10.78	92.96	18.69	936.00	455.92	7.77	5.22	20.35
C24016	240	74	17	1.6	11.48	92.91	19.78	1134.90	513.07	8.59	5.88	22.92
C24018	240	74	17	1.8	12.86	92.80	21.92	1612.70	635.62	10.26	7.28	28.37
C24020	240	74	17	2.0	14.23	92.70	23.99	2208.00	774.53	11.98	8.78	34.22
C24025	240	74	17	2.5	17.60	92.44	28.86	4291.70	1139.80	16.32	12.78	49.84
C24030	240	74	17	3.0	20.91	92.19	33.31	7380.00	1504.20	19.88	15.87	61.90
C30020	300	95	19	2.0	28.17	116.37	76.66	2773.30	783.54	20.51	11.15	43.48
C30025	300	95	19	2.5	34.92	116.11	92.96	5395.80	1172.90	28.65	16.65	64.93
C30030	300	95	19	3.0	41.55	115.85	108.19	9288.00	1626.50	37.25	22.94	89.46

Table 3. CFS back-to-back lipped-channel beam section, design variables and optimisation constraints

Back-to-back lipped channel section	Design variables	Constraints based on EC3	Comments	Manufacturing & practical limitations (mm)
	$x_1 = c/b$ $x_2 = b/L$	$0.2 \leq c/b \leq 0.6$ $b/t \leq 60$ $c/t \leq 50$ $h/t \leq 500$	EN1993-1-3 Table 5.1 and Equation (5.2a), Clause 5.5.3.2(1)	$400 \geq h \geq 100$ $b \geq 40$ $c \geq 10$

While the total plate width and plate thickness of each channel were kept constant during the optimisation process (to use the same amount of material as standard sections), the size optimisation was carried out following two different options to provide wider range of optimum cross-sections: (i) varying depth, flange width and lip length (fully optimised sections); (ii) varying depth and flange width while lip length is fixed the same as standard sections (partially optimised sections). The optimisation results for different UDLs and lengths are listed in Appendix I, and are discussed in detail in Section 6.

5.2 Frame optimisation

The structural level optimisation aimed to minimise the weight of the CFS portal frame per unit floor area (W) while satisfying all Eurocode design requirements. The unit weight depends on the frame spacing, frame geometry, cross-section sizes of the CFS members, and can be expressed as:

$$W = \frac{1}{L_f b_f} \left[\sum_{1}^{m} w_i l_i \right] \tag{18}$$

where W is the weight of the frame per square meter of floor area; L_f and b_f are the CFS portal frame span length and frame spacing, respectively; l_i and w_i are the length and the weight per unit length of the CFS frame members, respectively; and m is the number of structural members in the main frame.

In this study, the normalised forms of the member check provisions for CFS members following EC3 are used as optimisation constraints:

$$g_1 = \frac{N_{Ed}}{N_{t,Rd}} - 1 \leq 0 \tag{19-a}$$

$$g_2 = \frac{N_{Ed}}{N_{c,Rd}} - 1 \leq 0 \tag{19-b}$$

$$g_3 = \frac{N_{Ed}}{N_{b,Rd}} - 1 \leq 0 \tag{19-c}$$

$$g_4 = \frac{N_{Ed}}{N_{c,Rd}} + \frac{M_{y,Ed}}{M_{cy,Rd}} - 1 \leq 0 \qquad (19\text{-}d)$$

$$g_5 = \frac{M_{Ed}}{M_{b,Rd}} - 1 \leq 0 \qquad (19\text{-}e)$$

$$g_6 = \left(\frac{N_{Ed}}{N_{b,Rd}}\right)^{0.8} + \left(\frac{M_{Ed}}{M_{b,Rd}}\right)^{0.8} - 1 \leq 0 \qquad (19\text{-}f)$$

$$g_7 = \frac{\delta_e}{\delta_e^u} - 1 \leq 0 \qquad (19\text{-}g)$$

$$g_8 = \frac{\delta_a}{\delta_a^u} - 1 \leq 0 \qquad (19\text{-}h)$$

Where g_1, g_2 and g_3 are constraints for the axial members; g_4, g_5 and g_6 are constraints for the beam-column members; and g_7 and g_8 are constraints for the deflection limit checks. δ_e^u is the horizontal displacement limit at eaves; and δ_a^u is the vertical deflection limit at apex.

As discussed before, at the element level, a set of optimised CFS cross-sections with different coil widths and plate thicknesses are developed for the elements with various lengths subjected to different applied load (UDL) levels. Subsequently, at the frame level, the best cross-section (with minimum amount of material) are selected from the optimised sections to satisfy the design constraints imposed on the frame, based on the internal forces calculated at each iteration. The frame optimisation solver also searches through a practical range of values for the roof pitch, frame spacing, and knee brace configuration (i.e. knee depth and knee angle) to obtain the best design solution. This implies that at structural level optimisation, discrete and continuous design variables are simultaneously used. In this study, it is assumed that roof pitch is varied from 6° to 30° and frame spacing is set in the range of 2.0 m to 20 m.

5.3   Real-Coded Genetic Algorithm (RC-GA)

Due to the high nonlinearity of the optimisation problem in this study, a Real-Coded Genetic Algorithm (RC-GA) was programmed to solve the objective functions, including maximising the ultimate load-bearing capacity of CFS elements (Eq. 16) by satisfying the cross-sectional design constraints (see Table 3) and minimising the frame weight (Eq. 18) using the standard and optimised elements by considering all the predefined structural design constraints (Eqs. 19). It should be mentioned that RC-GA is a metaheuristic population-based algorithm, which is inspired by the natural selection and adaptation. The main advantage of RC-GA compared to conventional binary GA methods is that genetic operators are directly applied to the design variables without coding and decoding.

The adopted optimisation algorithm randomly generates a set of solutions known as initial population. From this population, the next generation of solutions is evolved by conducting three genetic operations: binary tournament selection, SBX crossover, and polynomial mutation [39, 40]. The process of random

selection in the binary tournament ensures that the best solutions in the population will not dominate the mating pool. The diversity of the population is thus preserved to increase the exploration component of the algorithm. To maintain the diversity of population when generation progresses, a niching technique is applied for selection and crossover operators. The details of this process can be found in Phan et al. [13].

To consider the design constraints for single objective optimisation in this study, an effective penalty approach [41, 42] is applied, in which the penalised value for each violated design constraint is gradually decreased as the generation progresses [33, 43]:

$$CVP_i = \frac{Ku_i}{Gen^{0.5}} \tag{20}$$

where CVP_i is the violated penalty for the ith design constraint, K is scale factor, u_i is the violated constraint, and Gen stands for the current generation. Since all design constraints are normalised to unity, an empirical scale factor of 100 was found to be sufficient to scale the penalty value to the same order with the objective function. Subsequently, the fitness function (F) in this study can be expressed as:

$$F = W(1 + \sum_{1}^{8} CVP_i) \tag{21}$$

As mentioned before, the adopted optimisation procedure aims to minimise the fitness function through evolutionary process to search for the lightest design that satisfies all design constraints. Specifically, for each solution, fitness function value is determined from objective function along with the penalty values for violated constraints. Better solutions will get smaller fitness values, and consequently, are selected preferentially by the tournament selection operator. The criterion for terminating the program is a predefined total number of generations.

To conduct optimisation process, the aforementioned design procedure in Section 3 and the Real-Coded Genetic Algorithm (RC-GA) were implemented in MATLAB [18]. The GA population size was taken equal to 50 and 80 for element and structural level optimisations, respectively; while the number of GA generations was kept 100 for both optimisation levels. The sensitivity analysis on the other GA parameters was also carried out, and subsequently the following values were selected: crossover probability p_c = 0.9; mutation probability p_m = 0.01; niching radius = 0.25; termination criterion = 100 generations (i.e. the maximum number of function evaluations allowed was 8000); distribution coefficient for mutation = 1.0; distribution coefficient for crossover = 1.0.

6 Results and discussions

In this study, a MATLAB code was developed to provide a link between ANSYS [22] and the RC-GA optimisation code. First, the results of element level optimisation conducted in MATLAB [18] were automatically transferred to ANSYS software [22] through an input file to develop the frame model. The element forces obtained from second-order elastic analysis were then recorded in an output file. Subsequently, the output data was transferred back to MATLAB [18] to carry out the optimisation process

at the frame level. The internal forces changed during the optimisation process by changing the size of the CFS structural elements. At each iteration, the new internal forces were then used to check the serviceability and ultimate limit states design conditions.

Although the optimisation process in this paper is based on Eurocode 3 design regulations, the proposed optimisation framework is general and other standards (e.g. AISI [44] and AS/NZS 4600 [45]) can be easily adopted. It should be mentioned that previous studies by the authors have also confirmed that the optimisation based on Eurocode 3 effective width method can accurately predict the actual trends in changing the capacity of CFS elements and hence lead to optimum design solutions [46-49].

6.1 Element level optimisation

For each CFS channel section listed in Table 2, the element level optimisation was repeated three times using different sets of random initial populations and the answer with the maximum bending capacity was retained as the optimum section. In all cases, the optimum solution was reasonably achieved with a consistently small standard deviation. For example, Fig. 6 shows the iteration history of the bending capacity for the C30020 beam (see Table 2) using back-to-back configuration, where the convergence was practically achieved after about 50 iterations. It should be noted that the cross-sections used in this study are all categorised as EC3 class 4 [19], and therefore, no yielding is expected before failure.
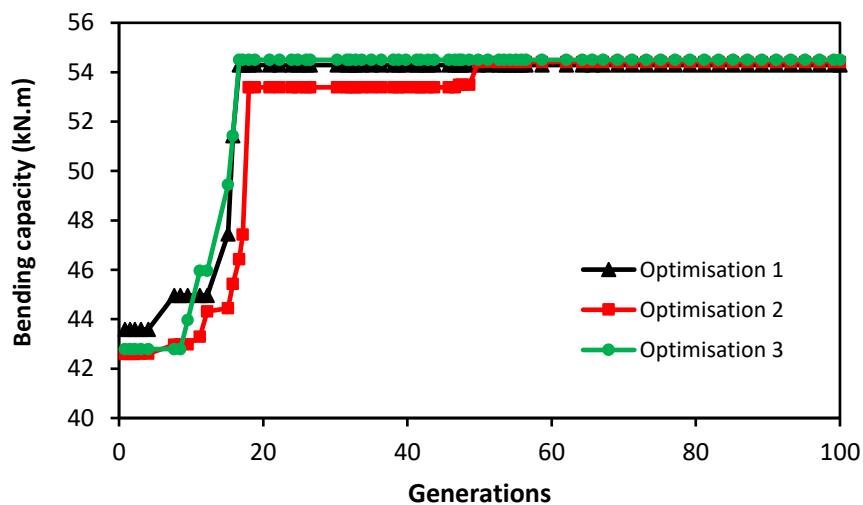
Fig. 6 Convergent history of element level optimisation for back-to-back channel using C30020 section

The comparison between the flexural capacities of the standard CFS sections and those optimised based on maximum bending moment capacity for 4 m length and different UDLs of 4, 6 and 8 kN/m are shown in Fig. 7 (a), (b), and (c), respectively. It can be seen that, for the same amount of material, the proposed optimisation method could significantly (up to 84%) increase the maximum bending capacity of the CFS beams with standard sections. It is also observed that optimising the lip length can result in a slight improvement (up to 8%) in the flexural capacity of the CFS beam members compared to the optimisation

using a fixed lip length (i.e. partially optimised sections). This minor difference can be attributed to the effect of lip length on the lateral-torsional buckling of the sections, which is taken into account through the buckling reduction factor (χ_{LT}) in the design process. It is worth mentioning that for the beams with small cross-sectional sizes and plate thickness (namely BBC14015, BBC17014, and BBC20014) standard sections cannot carry the large uniformly distributed loads (i.e. 6.0 kN/m and 8.0 kN/m), whilst the optimum sections provide enough capacity to sustain those design load levels. The optimum results for different element lengths and design load levels are listed in Appendix I. It should be noted that for those CFS beam sections which are not capable to satisfy the EC3 beam capacity design check (Eq. 17), no information is provided.
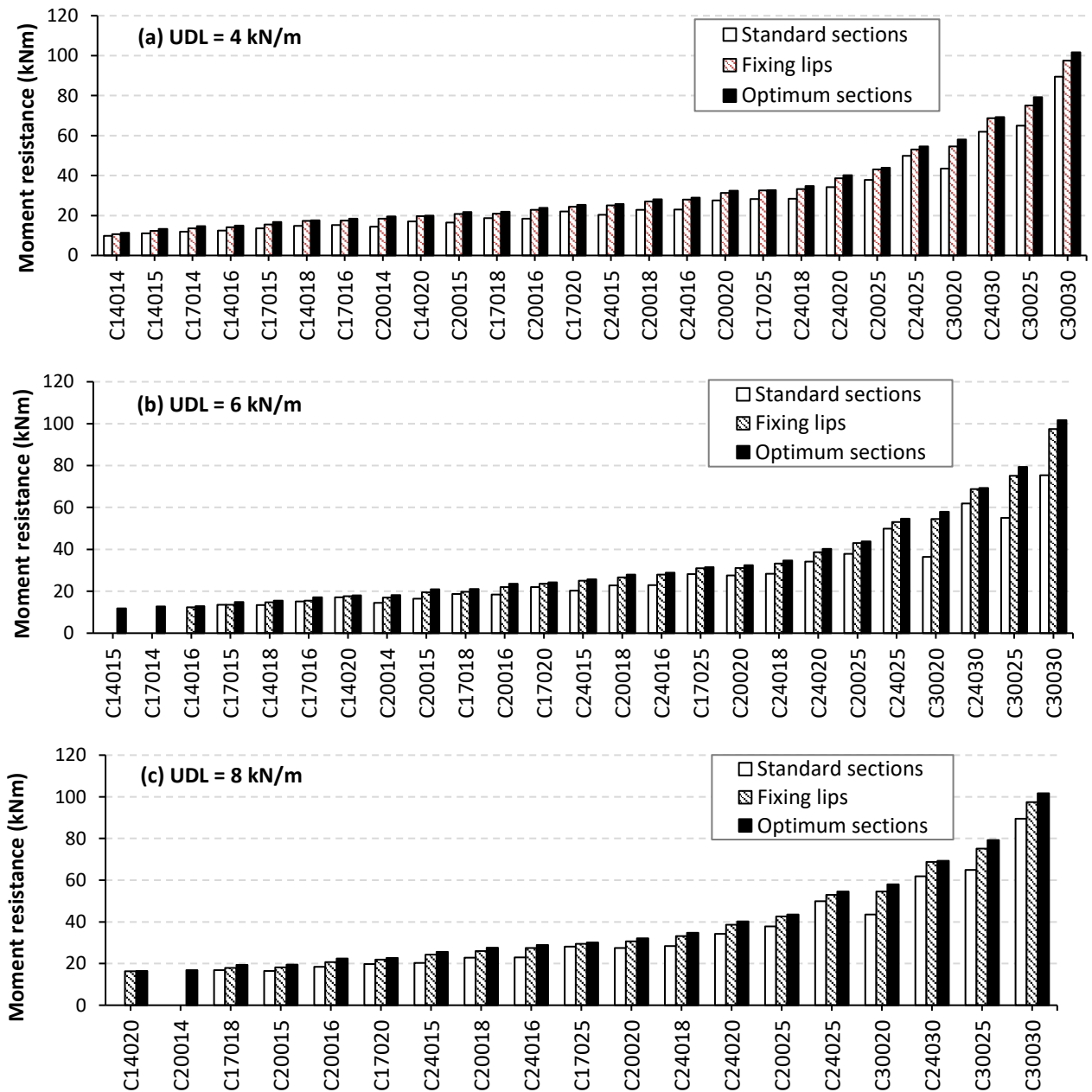

Fig. 7. Moment resistance of standard, partially optimised (fixed lip length) and fully optimised sections

18

6.2 Structural level optimisation

In this Section, the results of structural level optimisation on the selected CFS long-span portal frame with knee braces are presented by incorporating standard CFS back-to-back lipped-channel sections at two different limit state design conditions: (i) ULS, and (ii) combined ULS and SLS. For each case, the influence of optimising the frame geometry and knee brace configuration on the efficiency of the final solution is also investigated. All optimisation problems were conducted three times, and the answer with minimum structural weight was considered as the final optimum solution. In general, the standard deviation of the results was relatively small (less than 0.0058), which implies that the selected population size was sufficient. To obtain the internal forces and joint displacements for the structural level optimisation, second-order elastic analysis was conducted on the detailed FE models of the CFS frames using FE software ANSYS [22] (see Section 4). The results were then transferred to the RC-GA program in MATLAB as discussed in Section 5.

The selected CFS frame was initially optimised under ULS and combined ULS and SLS design conditions by using the most appropriate standard CFS elements (as listed in Table 2), while the initial geometry and knee brace configuration was assumed to be the same as the reference frame explained in Section 4. Subsequently, the frame was optimised again under ULS and combined ULS and SLS design conditions, but this time the frame geometry and knee brace configuration were also optimised. Table 4 compares the optimum results for all the above cases.

Table 4. Optimum design of the reference frame using CFS standard sections

Optimum design conditions	Knee brace configuration		Frame geometry		Member sections (back-to-back)			Unit weight (kg/m²)
	Knee depth (m)	Knee angle	Frame spacing (m)	Pitch	Column	Rafter	Knee brace	
Optimum design using reference frame geometry and knee brace configuration (ULS)	1.36	50º	3.60	10º	C-30030	C-30030	C-14015	12.75
Optimum design using reference frame geometry and knee brace configuration (ULS & SLS)	1.36	50º	3.60	10º	N/A	N/A	N/A	N/A
Optimum design (ULS)	1.87	40.1º	4.30	6.0º	C-30030	C-30030	C-14015	10.62
Optimum design (ULS & SLS)	1.40	52.8º	2.21	6.0º	C-30030	C-30030	C-14015	20.63

The optimum weight of the frame optimised under ULS using the geometry of the reference frame was calculated 12.75 kg per square meter of floor area (kg/m²) by using the strongest cross-section available in Table 2 for rafters and columns (C-30030) and standard section C-14015 for knee brace members. In this case, the design constraint related to the lateral-torsional buckling of the column members under bending and compression interaction (g_6) governed the design (i.e. g_6=0 under the critical load combination LC3). As

can be seen in Table 4, when the geometry of the frame is not optimised, no optimum solution is obtained under combined ULS and SLS conditions. The reason is that none of the standard sections used in this study (Table 2) can satisfy the predefined design constraint on the horizontal displacement at eaves (SLS load combination LC5).

As mentioned above, the selected CFS long-span portal frame was also optimised by including the frame geometry (i.e. frame spacing and pitch angle) and knee brace configuration (i.e. knee depth and knee angle) in the optimisation process. The most suitable standard cross-sections were obtained to provide the lightest solution by considering the design constraints at ULS and combined ULS and SLS. The results in Table 4 indicate that, by optimising the frame geometry and knee brace configuration, the required structural weight for ULS design reduced by 17%, while the frame spacing was increased from 3.60 m to 4.30 m. Similar to the previous case, the optimum result at ULS was controlled by the design constraint on the lateral-torsional buckling of the column members under bending and compression interaction (i.e. g_6=0 under the critical load combination LC3). Incorporating the optimum knee brace configuration and frame geometry enabled the frame designed at combined ULS and SLS to satisfy the horizontal displacement constraint at eaves (i.e. g_7=0 under the critical load combination LC5). This led to a considerable increase in the required structural weight compared to the frame optimised at ULS, which indicates that the serviceability design conditions governed the design as expected for the long-span frame considered in this study. The results in Table 4 also demonstrate that the optimum design solution always tends to provide larger knee brace depth (up to 38%) regardless of the selected limit state design conditions. On the contrary, the optimum knee brace angle is affected by the selected limit state design condition, since changing the knee brace angle can also change the bending moment in the rafters and, hence, affect the frame displacement.

6.3 Coupled element and structural level optimisation

This section presents the structural level optimisation are carried out on the selected CFS long-span portal frame with knee braces by incorporating optimised CFS lipped-channel sections at two different limit state design conditions: (i) ULS, and (ii) combined ULS and SLS. To examine the efficiency of the CFS sections optimised at element level (see Section 6.1) for structural level optimisation, the reference CFS frame was optimised again by using optimum CFS sections instead of the standard elements (i.e. coupled element and structural level optimisation). Table 5 compared the optimum design solutions under ULS and combined ULS and SLS conditions with and without optimising the frame geometry and knee brace configuration.

Table 5. Optimum design of the reference frame using optimised sections

Optimum design conditions	Knee brace configuration		Frame geometry		Member sections (back-to-back)			Unit weight (kg/m²)
	Knee depth (m)	Knee angle	Frame spacing (m)	Pitch	Column	Rafter	Knee brace	

Optimum design using reference frame geometry and knee brace configuration (ULS)	1.36	50°	3.60	10°	C-30030*	C-30025*	C-20015*	11.85
Optimum design using reference frame geometry and knee brace configuration (ULS & SLS)	1.36	50°	3.60	10°	N/A	N/A	N/A	N/A
Optimum design (ULS)	1.85	40.5°	4.55	6.0°	C-30030*	C-30030*	C-20015*	10.19
Optimum design (ULS & SLS)	1.40	52.7°	2.77	6.0°	C-30030*	C-30030*	C-14014*	16.42

* Elements with optimum dimensions as indicated in Appendix I

Similar to the previous case, the critical design constraints were the lateral-torsional buckling of the column members (g_6) and horizontal displacement at eaves (g_7) under ULS and combined ULS and SLS design conditions, respectively. The CFS frame with the geometry and knee brace configuration similar to the reference experimental test could not satisfy the serviceability design conditions, while full optimisation could reduce the required structural weight for ULS design by 14%.

Comparison between the results in Tables 4 and 5 indicates that by using optimised CFS elements the required structural weight was reduced by up to 20% compared to the frame optimised using the standard elements listed in Table 2. The material saving due to using optimised CFS sections was especially evident when the frame was optimised under combined ULS and SLS design conditions. It is also shown that using optimised sections in general results in a higher frame spacing (up to 25%), while it does not considerably affect the optimum knee brace configuration (i.e. knee depth and knee angle).

7 Summary and conclusions

A novel coupled element and structural level optimisation framework was presented for optimum design of CFS portal frames under different limit state design conditions. To search for the optimum design solutions, a Real-Coded Genetic Algorithm (RC-GA) was adopted, in which the genetic operators were directly applied to the design variables without coding and decoding. In the proposed framework, first the relative dimensions of a wide range of standard CFS lipped-channel sections were optimised with respect to their flexural capacity determined according to the Eurocode-3 effective width method, while the EC3 slenderness limits and a number of manufacturing and end-use constraints were considered in the optimisation process. It was shown that, by using the same amount of material, the ultimate flexural capacity of the optimum CFS members can be significantly higher (up to 84%) than their standard counterparts. Subsequently, structural level optimisation was conducted on a long-span CFS portal frame with knee braces under SLS and ULS conditions to find the best economic design with the lightest weight per unit area using both standard and optimised cross-sections. The results indicated that the proposed coupled framework can considerably reduce (up to 20%) the required structural weight of the CFS frame system by using the CFS sections optimised for generic applications. It was also shown that optimising the frame geometry and knee brace configuration, could further reduce the structural weight (up to 17%),

especially under combined ULS and SLS design conditions. Based on the outcomes of this study, the proposed coupled optimisation framework should prove useful in practical design of CFS frame systems.

References

[1] H. Adeli, A. Karim, Neural network model for optimization of cold-formed steel beams, J. Struct. Eng. ASCE 123, (1997) 1535–1543.

[2] A. Karim, H. Adeli, Global optimum design of cold-formed steel hat-shape beams, Thin-Walled Structures, 35 (1999) 275-288.

[3] J. Ye, I. Hajirasouliha, J. Becque, K. Pilakoutas, Development of more efficient cold-formed steel channel sections in bending, Thin-Walled Structures, 101 (2016) 1-13.

[4] J. Ye, I. Hajirasouliha, J. Becque, A. Eslami, Optimum design of cold-formed steel beams using Particle Swarm Optimisation method, Journal of Constructional Steel Research, 122 (2016) 80-93.

[5] B.P. Gilbert, T.J.M. Savoyat, L.H. Teh, Self-shape optimisation application: Optimisation of cold-formed steel columns, Thin-Walled Structures, 60 (2012) 173-184.

[6] B. Wang, G.L. Bosco, B.P. Gilbert, H. Guan, L.H. Teh, Unconstrained shape optimisation of singly-symmetric and open cold-formed steel beams and beam-columns, Thin-Walled Structures, 104 (2016) 54-61.

[7] J. Leng, J.K. Guest, B.W. Schafer, Shape optimization of cold-formed steel columns, Thin-Walled Structures, 49 (2011) 1492-1503.

[8] J. Leng, Z. Li, J.K. Guest, B.W. Schafer, Shape optimization of cold-formed steel columns with fabrication and geometric end-use constraints, Thin-Walled Structures, 85 (2014) 271-290.

[9] T. Tran, L.-y. Li, Global optimization of cold-formed steel channel sections, Thin-Walled Structures, 44 (2006) 399-406.

[10] S.M. Mojtabaei, J. Ye, I. Hajirasouliha, Development of optimum cold-formed steel beams for serviceability and ultimate limit states using Big Bang-Big Crunch optimisation, Engineering Structures, 195 (2019) 172-181.

[11] H. Parastesh, I. Hajirasouliha, H. Taji, A. Bagheri Sabbagh, Shape optimization of cold-formed steel beam-columns with practical and manufacturing constraints, Journal of Constructional Steel Research, 155 (2019) 249-259.

[12] J. Ye, J. Becque, I. Hajirasouliha, S.M. Mojtabaei, J.B.P. Lim, Development of optimum cold-formed steel sections for maximum energy dissipation in uniaxial bending, Engineering Structures, 161 (2018) 55-67.

[13] D.T. Phan, J.B.P. Lim, T.T. Tanyimboh, W. Sha, An efficient genetic algorithm for the design optimization of cold-formed steel portal frame buildings, Steel and Composite Structures, An International Journal, 15(5) (2013) 519-538.

[14] D.T. Phan, J.B.P. Lim, W. Sha, C. Siew, T.T. Tanyimboh, K.H. Issa, F.A. Mohammad, Design optimization of cold-formed steel portal frames taking into account the effect of topography, Engineering Optimization, 45 (2013) 415-433.

[15] D.T. Phan, J.B.P. Lim, T.T. Tanyimboh, A.M. Wrzesien, W. Sha, R.M. Lawson, Optimal design of cold-formed steel portal frames for stressed-skin action using genetic algorithm, Engineering Structures, 93 (2015) 36-49.

[16] R. McKinstray, J.B.P. Lim, T.T. Tanyimboh, D.T. Phan, W. Sha, Optimal design of long-span steel portal frames using fabricated beams, Journal of Constructional Steel Research, 104 (2015) 104-114.

[17] D.T. Phan, J.B.P. Lim, T.T. Tanyimboh, R.M. Lawson, Y. Xu, S. Martin, W. Sha, Effect of serviceability limits on optimal design of steel portal frames, Journal of Constructional Steel Research, 86 (2013) 74-84.

[18] Mathworks, Matlab R2011a, in, Mathworks, Inc, 2011.

[19] CEN, Eurocode 3: Design of Steel Structures. Part 1-1: General Rules and Rules for Buildings, in, Brussels: European Comittee for Standardization, (2005).

[20] CEN, Eurocode 3: design of steel structures, part 1.3: general rules—supplementary rules for cold formed members and sheeting, in, Brussels: European Comittee for Standardization, (2005).

[21] CEN, Eurocode 3: Design of steel structures, Part 1-5: Plated structural elements, in, Brussels: European Comittee for Standardization, (2006).

[22] ANSYS Inc., Programmer's manual for mechanical APDL. USA: SAS IP, (2009).

[23] F.J. Meza, J. Becque, I. Hajirasouliha, Experimental study of cold-formed steel built-up columns, Thin-Walled Structures (in press), (2019).

[24] BS EN 1991-1-1, Eurocode 1, Actions on structures: Part 1-1 General actions, Densities, self-weight, imposed loads for buildings, Incorporating corrigendum No. 1, BSI, (2002).

[25] D.M. Koschmidder, D.G. Brown, Elastic design of single span steel portal frame buildings to Eurocode 3, SCI Publication P397, Berkshire UK, (2012).

[26] BS EN 1991-1-4, Eurocode 1, Actions on structures: Part 1-4 General actions, Wind actions. BSI, 2005, (2005).

[27] CEN, Eurocode 0: "Basis of structural design." , European Committee for Standardization, Brussels, (2002).

[28] SCI Advisory Desk, AD-090: Deflection limits for pitched roof portal frames (Amended), Ascot: The Steel Construction Institute, (2010).

[29] H.B. Blum, Long-span cold-formed steel portal frames composed of double channels. PhD Thesis. The University of Sydney, Australia, (2016).

[30] H.B. Blum, K.J.R. Rasmussen, Experimental investigation of long-span cold-formed steel double channel portal frames, Journal of Constructional Steel Research, 155 (2019) 316-330.

[31] J. Peng, J. Bendit, H.B. Blum, Experimental Study of Apex Connection Stiffness and Strength of Cold-Formed Steel Double Channel Portal Frames, International Specialty Conference on Cold-Formed Steel Structures, (2018).

[32] A. Wreszien, J.B.P. Lim, D.A. Nethercot, Optimum joint detail for a general cold-formed steel portal frame, Advances in Structural Engineering, Advances in Structural Engineering, 15 (2012) 1623-1639.

[33] D.T. Phan, J.B.P. Lim, S.J. Meheron, H.H. Lau, Design Optimization of Long-Span Cold-Formed Steel Portal Frames Accounting for Effect of Knee Brace Joint Configuration, Technologies (MDPI), 5(81) (2017) 1-13.

[34] J.B.P. Lim, D.A. Nethercot, Ultimate strength of bolted moment-connections between cold-formed steel members, Thin Wall Structures, 41 (2003) 1019-1039.

[35] J.B.P. Lim, D.A. Nethercot, Finite element idealization of a cold-formed steel portal frame, Journal of Structural Engineering, 130 (2004) 78-94.

[36] J.B.P. Lim, G.J. Hancock, G.C. Clifton, C.H. Pham, R. Das, DSM for ultimate strength of bolted moment-connections between cold-formed steel channel members, Journal of Constructional Steel Research, 117 (2016) 196-203.

[37] S.M. Mojtabaei, M.Z. Kabir, I. Hajirasouliha, M. Kargar, Analytical and experimental study on the seismic performance of cold-formed steel frames, Journal of Constructional Steel Research, 143 (2018) 18-31.

[38] D.T. Phan, J.B.P. Lim, T.T. Tanyimboh, W. Sha, Optimum design of cold-formed steel portal frame buildings including joint effects and secondary members, International Journal of Steel Structures, 17(2) (2017) 427-442.

[39] K. Deb, Multi-objective optimization using evolutionary algorithms. Chichester: John Wiley and Sons, Inc., (2001).

[40] K. Lwin, R. Qu, G. Kendall, A learning-guided multi-objective evolutionary algorithm for constrained portfolio optimization, Applied Soft Computing, 24 (2014) 757-772.

[41] S. Pezeshk, C.V. Camp, D. Chen, Design of Nonlinear Framed Structures Using Genetic Optimization, Journal of Structural Engineering, 126 (2000) 382-388.

[42] O. Yeniay, Penalty function methods for constrained optimization with genetic algorithms. , Mathematical and Computational Applications, 10(1) (2005) 45-56.

[43] F. Erbatur, O. Hasançebi, İ. Tütüncü, H. Kılıç, Optimal design of planar and space structures with genetic algorithms, Computers & Structures, 75 (2000) 209-224.

[44] AISI S100-16, North American specification for the design of cold-formed steel structural members. , American Iron and Steel Institute (AISI), Washington, DC, USA, (2016).

[45] AS/NZS 4600:2018, Coldformed steel structures, Homebush, Australia, Standards Australia/Standards New Zealand (SA/SNZ).

[46] J. Ye, F.J. Meza, I. Hajirasouliha, J. Becque, P. Shepherd, K. Pilakoutas, Experimental Investigation of Cross-Sectional Bending Capacity of Cold-Formed Steel Channels Subject to Local-Distortional Buckling Interaction, Journal of Structural Engineering, 145 (2019) 04019064.

[47] J. Ye, I. Hajirasouliha, J. Becque, Experimental investigation of local-flexural interactive buckling of cold-formed steel channel columns, Thin-Walled Structures, 125 (2018) 245-258.

[48] J. Ye, S.M. Mojtabaei, I. Hajirasouliha, P. Shepherd, K. Pilakoutas, Strength and deflection behaviour of cold-formed steel back-to-back channels, Engineering Structures, 177 (2018) 641-654.

[49] J. Ye, S.M. Mojtabaei, I. Hajirasouliha, Local-flexural interactive buckling of standard and optimised cold-formed steel columns, Journal of Constructional Steel Research, 144 (2018) 106-118.

Appendix I

Table A. Cross-section dimensions of standard and optimised CFS lipped-channel sections under 4, 6 and 8 kN/m uniformly distributed loads, 4 m span length

Section	Standard depth (mm)	Optimum depth (mm)			Standard width (mm)	Optimum width (mm)			Standard lip (mm)	Optimum lip (mm)			Standard I_{eff} (mm⁴)	Optimum I_{eff} (mm⁴)		
		UDL 4	ULD 6	UDL 8		UDL 4	ULD 6	UDL 8		UDL 4	ULD 6	UDL 8		UDL 4	ULD 6	UDL 8
C14014	140	144.04	-	-	62	50.95	-	-	13	22.03	-	-	2054000	2306400	-	-
C14015	140	148.11	156.72	-	62	49.62	45.44	-	13	21.33	21.19	-	2274000	2686500	2957471	-
C14016	140	151.13	136.22	-	62	48.02	48.63	-	13	21.41	28.26	-	2497600	3031200	2477226	-
C14018	140	159.26	133.54	-	62	47.24	56.58	-	13	18.13	21.65	-	2896100	3727000	2772600	-
C14020	140	164.05	142.01	157.98	62	45.36	55.39	48.11	13	17.62	18.61	17.9	3289800	4339700	3437800	4089800
C17014	170	181.73	189.21	-	62	46.08	43.01	-	13	23.05	22.39	-	3098500	3784200	4061300	-
C17015	170	186.09	162.64	-	62	45.38	54.5	-	13	21.58	24.19	-	3435200	4343000	3416900	-
C17016	170	188.16	166.71	-	62	44.13	53.18	-	13	21.79	23.46	-	3777400	4760100	3931400	-
C17018	170	189.7	172.46	155.11	62	44.13	50.3	58.4	13	21.02	23.47	24.04	4475200	5529300	4832400	4037600
C17020	170	191.02	180.67	164.04	62	44.13	49.92	57.44	13	20.36	19.74	20.54	5138600	6316700	5810300	4979900
C17025	170	202.82	190.76	176.25	62	44.13	45.95	52.58	13	14.46	18.67	19.3	6476000	8572800	7877600	6983800
C20014	200	243.1	219.37	202.72	70	42.14	48.32	55.2	15	21.31	26.99	28.44	4585100	6944400	5884800	5081200
C20015	200	243.38	223.41	207.27	70	40	47.25	53.87	15	23.31	26.04	27.49	5099700	7612800	6733800	5886500
C20016	200	238.69	228.81	211.26	70	41.03	47.25	52.73	15	24.62	23.35	26.65	5624300	8058900	7637500	6713400
C20018	200	242.01	230.52	216.23	70	40	43.59	49.69	15	24	26.15	27.2	6698700	9423100	8883400	8166000
C20020	200	242.01	235.38	220.36	70	40	42.07	47.29	15	24	25.24	27.53	7799700	10679000	10325000	9479600
C20025	200	240.95	240.95	235.34	70	43.66	43.66	45.99	15	20.87	20.87	21.34	10266000	13827000	13827000	1341000
C24015	240	277.35	277.35	272.36	74	50	50	50	17	22.33	22.33	24.82	7771200	10652000	10652000	10408000
C24016	240	276.86	276.86	276.86	74	50	50	50	17	22.57	22.57	22.57	8586400	11726000	11726000	11726000
C24018	240	267.74	267.72	267.74	74	50	50	50	17	27.13	27.14	27.13	10260000	13137000	13137000	13137000
C24020	240	261.98	261.98	261.98	74	50	50	50	17	30.01	30.01	30.01	11980000	14510000	14510000	14510000
C24025	240	266.05	266.05	266.05	74	50	50	50	17	27.98	27.98	27.98	16322000	19261000	19261000	19261000
C24030	240	283.22	283.22	283.22	74	50	50	50	17	19.39	19.39	19.39	19878000	25614000	25614000	25614000
C30020	300	362.25	362.25	362.25	95	51.8	51.8	51.8	19	31.05	31.05	31.05	20506000	30424000	30424000	30424000
C30025	300	342.48	342.48	342.48	95	57.97	57.97	57.97	19	34.78	34.78	34.78	28645000	37479000	37479000	37479000
C30030	300	342.91	342.91	342.91	95	58.82	58.82	58.82	19	33.73	33.73	33.73	37247000	46599000	46599000	46599000

Table B. Cross-section dimensions of standard and optimised CFS lipped-channel sections under 4, 6 and 8 kN/m uniformly distributed loads, 6 m span length

Section	Standard depth (mm)	Optimum depth (mm)			Standard width (mm)	Optimum width (mm)			Standard lip (mm)	Optimum lip (mm)			Standard I_{eff} (mm^4)	Optimum I_{eff} (mm^4)		
		UDL 4	ULD 6	UDL 8		UDL 4	ULD 6	UDL 8		UDL 4	ULD 6	UDL 8		UDL 4	ULD 6	UDL 8
C17018	170	168.52	-	-	62	52.32	-	-	13	23.42	-	-	4475200	4672000	-	-
C17020	170	156.24	-	-	62	60.99	-	-	13	20.89	-	-	5138600	4589400	-	-
C17025	170	169.45	-	-	62	55.68	-	-	13	19.59	-	-	6476000	6565600	-	-
C20015	200	199.82	-	-	70	56.98	-	-	15	28.11	-	-	5099700	5501600	-	-
C20016	200	204.11	-	-	70	55.69	-	-	15	27.26	-	-	5624300	6308400	-	-
C20018	200	211.13	-	-	70	53.21	-	-	15	26.23	-	-	6698700	7902600	-	-
C20020	200	214.77	190.47	-	70	50.17	61.38	-	15	27.44	28.38	-	7799700	9155600	7697700	-
C20025	200	229.9	207.92	188.62	70	48.47	58.42	67.19	15	21.58	22.62	23.5	10266000	12966000	11152000	9539000
C24015	240	261.06	-	-	74	50.39	-	-	17	30.08	-	-	7771200	9773600	-	-
C24016	240	266.48	-	-	74	50	-	-	17	27.76	-	-	8586400	11130000	-	-
C24018	240	267.74	248.66	-	74	50	56.84	-	17	27.13	29.83	-	10260000	13137000	11770000	-
C24020	240	261.98	253.02	236.96	74	50	53.89	62.58	17	30.01	30.6	29.94	11980000	14510000	13873000	12595000
C24025	240	266.05	265.6	258.33	74	50	50.13	56.38	17	27.98	28.06	25.46	16322000	19261000	19222000	17568000
C24030	240	283.22	279.58	262.67	74	50	50	55.24	17	19.39	21.21	24.43	19878000	25614000	25212000	23121000
C30020	300	362.25	362.25	360.82	95	51.8	51.8	52.69	19	31.08	31.08	30.89	20506000	30424000	30424000	30281000
C30025	300	342.48	342.48	342.48	95	57.97	57.97	57.97	19	34.78	34.78	34.78	28645000	37479000	37479000	37479000
C30030	300	342.91	342.91	342.91	95	58.82	58.82	58.82	19	33.73	33.73	33.73	37247000	46599000	46599000	46599000

Table C. Cross-section dimensions of standard and optimised CFS lipped-channel sections under 4, 6 and 8 kN/m uniformly distributed loads, 8 m span length

Section	Standard depth (mm)	Optimum depth (mm)			Standard width (mm)	Optimum width (mm)			Standard lip (mm)	Optimum lip (mm)			Standard I_{eff} (mm^4)	Optimum I_{eff} (mm^4)		
		UDL 4	ULD 6	UDL 8		UDL 4	ULD 6	UDL 8		UDL 4	ULD 6	UDL 8		UDL 4	ULD 6	UDL 8
C20025	200	197.01	-	-	70	63.38	-	-	15	23.12	-	-	10266000	10238000	-	-
C24015	240	-	-	-	74	-	-	-	17	-	-	-	7771200	-	-	-
C24016	240	-	-	-	74	-	-	-	17	-	-	-	8586400	-	-	-
C24018	240	237.49	-	-	74	61.44	-	-	17	30.81	-	-	10260000	10847000	-	-
C24020	240	245.09	-	-	74	59.38	-	-	17	29.08	-	-	11980000	13286000	-	-
C24025	240	254.57	233.83	-	74	53.21	67.14	-	17	30.5	26.94	-	16322000	18175000	16171000	-
C24030	240	268.79	245.56	-	74	52.45	63	-	17	24.15	25.21	-	19878000	23906000	20944000	-
C30020	300	362.25	345.94	-	95	51.8	60.56	-	19	31.08	30.47	-	20506000	30424000	28742000	-
C30025	300	342.48	342.48	334.71	95	57.97	57.97	60.4	19	34.78	34.78	36.24	28645000	37479000	37479000	36451000
C30030	300	342.91	342.91	342.91	95	58.82	58.82	58.82	19	33.73	33.73	33.73	37247000	46599000	46599000	46599000